university of groningen

University Medical Center Groningen

University of Groningen

Biophysical Interactions of vaginal microorganisms

Younes, Jessica Anne

IMPORTANT NOTE: You are advised to consult the publisher's version (publisher's PDF) if you wish to cite from it. Please check the document version below.

Document Version
Publisher's PDF, also known as Version of record

Publication date:
2015

Link to publication in University of Groningen/UMCG research database

Citation for published version (APA):
Younes, J. A. (2015). *Biophysical Interactions of vaginal microorganisms*. [Thesis fully internal (DIV), University of Groningen]. University of Groningen.

Copyright
Other than for strictly personal use, it is not permitted to download or to forward/distribute the text or part of it without the consent of the author(s) and/or copyright holder(s), unless the work is under an open content license (like Creative Commons).

The publication may also be distributed here under the terms of Article 25fa of the Dutch Copyright Act, indicated by the "Taverne" license. More information can be found on the University of Groningen website: https://www.rug.nl/library/open-access/self-archiving-pure/taverne-amendment.

Take-down policy
If you believe that this document breaches copyright please contact us providing details, and we will remove access to the work immediately and investigate your claim.

Downloaded from the University of Groningen/UMCG research database (Pure): http://www.rug.nl/research/portal. For technical reasons the number of authors shown on this cover page is limited to 10 maximum.

Download date: 06-05-2023

Chapter 5

Vaginal Epithelial Cells Create Sticky Membranes for Bacterial Binding

Manuscript in preparation for Nature Letters. Jessica A. Younes, Karin Klappe, Jan Willem Kok, Henk J. Busscher , Gregor Reid, & Henny C. van der Mei.

Abstract

Vaginal biofilms are important in both health and disease, depending on their bacterial composition. Adhesion of bacteria to vaginal epithelial cells is a crucial first step in biofilm formation. Although many bacterial species can be detected in this niche[1], little is known about the relative contribution of epithelial and bacterial cell surfaces to these adhesive events and how the cumulative binding events are coordinated at the level of the epithelial cell membrane. Here we quantitatively show and compare how 'sticky' the vaginal epithelial membrane is above the cytoplasm and nucleus for different members of the vaginal microbiota. The adhesion force between the bacteria and the epithelial cell membrane above the cytoplasm was consistently stronger than on the membrane above the nucleus both for vaginal pathogens as well as for commensal and probiotic lactobacillus strains involved in health, suggesting an active cellular mechanism. We provide mechanistic evidence of the direct role that membrane cholesterol and sub-membrane actin play in initial bacterial membrane adhesion by using depletion of cholesterol (MβCD) and actin inhibitors (Latrunculin B), yielding an enormous decrease in adhesion forces. Our results demonstrate that vaginal epithelial cells actively modulate bacterial adhesion and determine where the bacterium can start initial biofilm formation.

Main Text

In the vagina, epithelial cells and vaginal bacteria interact via adhesion for multiple purposes, ranging from mutualism and commensalism to invasion and parasitism[2]. Adhesion to the target surface accomplishes the first step in biofilm formation in order for a microorganism to reside. Bacterial evolution has resulted in a wide array of adhesive molecules that permit them to exploit a large number of cellular surface receptors[3]. The cell is also highly attractive as an adhering surface because it offers bacteria protection, nutrition and synergistic advantages. However, it is unclear whether the initial binding events at the vaginal epithelium are regulated equally by both bacteria and cells.

To directly investigate the global 'stickiness' of bacteria to the vaginal epithelium, vaginal VK2/E6E7 cells were incubated with monocultures of six bacterial strains representative of genera common to the vagina. Our selection of bacterial strains included Gram-positive and Gram-negative strains, a range of shapes (cocci, normal and pleomorphic rods), and bacteria with varying roles in the vaginal microbiota (pathogens, commensals, probiotics); this was intended to assess differences in adhesion. Three pathogenic strains and three lactobacilli were used: *Escherichia coli* C1214, *Staphylococcus aureus* MN8, *Gardnerella vaginalis* BME-1, *Lactobacillus iners* AB-1, *Lactobacillus crispatus* 33820, and *Lactobacillus reuteri* RC-14. The numbers of membrane-adhered bacteria in embedded cross-sectioned samples were quantified over two cell locations, the membrane above the nucleus and above the cytoplasm. Initial bacterial cohesion or aggregation that would eventually build up and form biofilms

was observed on the cells (Figure 1A, B). More bacteria adhered on the membrane above the cytoplasm (Figure 1C) than on the membrane above the nucleus with an average ratio of 1.97. This consistent trend of preferential adhesion to the membrane above the cytoplasm for all bacterial strains suggested that the cells had a larger contribution to initial adhesion than bacteria.

To investigate whether the differences between bacterial strains was due to differences in the adhesion force of the strains, we performed atomic force microscopy (AFM) adhesion force measurements. This sensitive technique permitted us to quantify interactions[4] between a bacterial probe to different membrane locations on a VK2/E6E7 cell. By ruling out any confounding or contributing effects of cohesion and aggregation of the bacteria toward adhesion to the cells, we could directly measure adhesion forces between a bacterium and the VK2/E6E7 cellular membrane. Adhesion forces to the membrane above the cytoplasm were twice as strong as to the membrane above the nucleus for all six bacterial strains (Figure 1C). The differences in adhesion forces are most clearly expressed at 120 s (Figure 1D, E). For instance, G*. vaginalis* BME-1 adhered to the membrane above cytoplasm with -11.9 ± 0.4 nN versus -5.7 ± 0.4 nN above the nucleus, while *L. crispatus* 33280 adhered above the cytoplasm with -10.1 ± 0.3 nN and above the nucleus with -6.0 ± 0.3 nN. Liu, *et al*. measured 9.3 ± 2.4 nN adhesion of *E. coli* to uroepithelial cells and our results are consistent with the order of magnitude shown in their study[5].

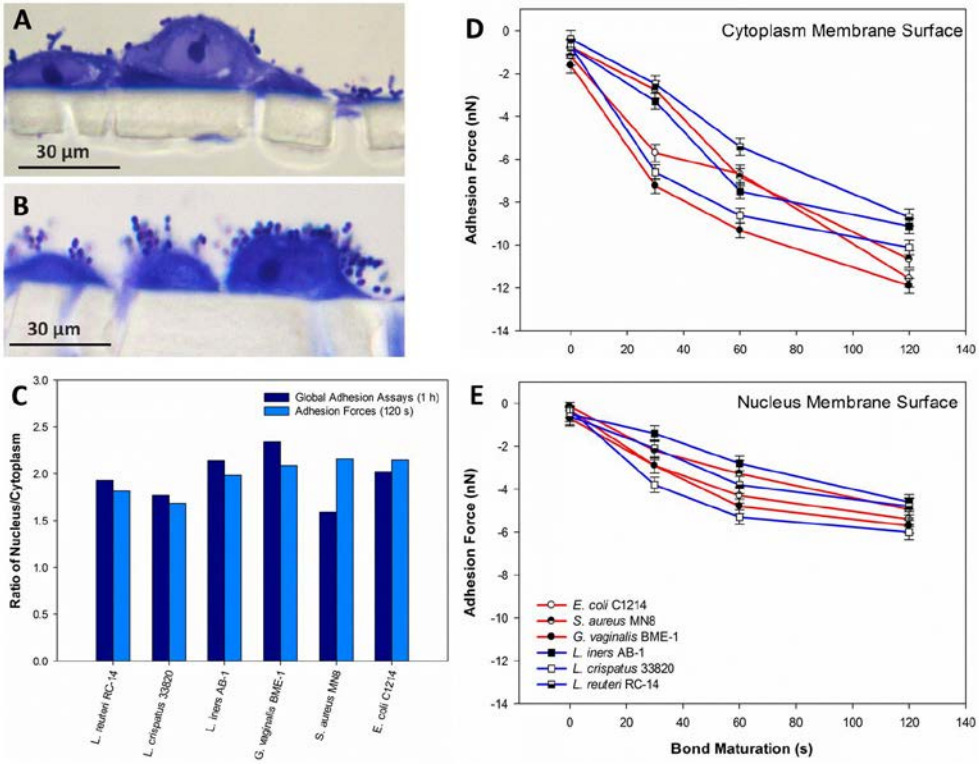

Figure 1 | Quantification of embedded and cross-sectioned bacterial adhesion assays and bacterial adhesion forces between VK2/E6E7 cells and vaginal microbiota strains.

A | A toluidine blue-stained cross-section of embedded and fixated VK2/E6E7 epithelial cells exposed to *L. reuteri* RC-14 (1.0 x 10^5 bacteria/mL) for 1 h.

B | Shows a cross-section of *S. aureus* MN8 on VK2/E6E7 cells under the same conditions as in **A**.

C | Ratios of the numbers of adhering bacteria (dark blue columns) and their adhesion forces at 120 s (light blue columns) were calculated by dividing the number of adhering bacteria on the membrane above the cytoplasm of the cell by the number of bacteria adhering to the membrane above the nucleus of the cell or in the case of adhesion forces the adhesion force above the cytoplasm divided by the adhesion force above the nucleus. A value greater than 1 indicates that the particular bacterial strain adheres in higher numbers or has stronger adhesion forces to the membrane above the cytoplasm than the nucleus. Individual adhesion assay data are an average of the quantified bacteria adhered to between 80-150 cells, within 3 separate cell passages and using at least 3 different bacterial cultures. Individual adhesion force data are an average of 30 force-distance curves measured on at least 6 different epithelial cells using three bacterial probes prepared from at least two different bacterial cultures per strain.

D | Adhesion forces as a function of bond-maturation time for the membrane region above the cytoplasmic space. AFM adhesion force data represent averages over at least 30 force-distance curves, measured on at least 6 different epithelial cells by three different bacterial probes with at least two different cultures per strain. All bacteria were significantly different ($p<0.05$) from each other at 120 s with the exception of the pairs *S. aureus* MN8-*L. crisptaus* 33820 and *L. reuteri* RC-14-*L. iners* AB-1.
E | Same as **D** for the membrane region above the nucleus. All bacteria were significantly different ($p<0.05$) from each other at 120 s with the exception of the following pairs: *G. vaginalis* BME-1 with *S. aureus* MN8, *E. coli* C1214, *L. iners* AB-1 and *L. crisptaus* 33820; *S. aureus* MN8 with *E. coli* C1214, *L. iners* AB-1, and *L. reuteri* RC-14; *E. coli* C1214 with *L. iners* AB-1, and *L. reuteri* RC-14; *L. iners* AB-1 with *L. reuteri* RC-14; *L. iners* AB-1 with *L. crisptaus* 33820.

Of note, the epithelial cell was more adhesive to the pathogens (red lines; Figure 1D, E) than to the lactobacilli (blue lines). Though little is known about the order of bacterial colonization in the vagina, phylogenic research does show the higher abundance of certain species associated with health or disease[1]. *G. vaginalis* is considered to be an important colonizer in bacterial vaginosis[6,7], partially because of its resilient ability to remain even amid the presence of lactobacilli[7], and also due to its symbiotic interactions with pathogen[6]. This idea is further supported by the strong adhesion forces shown in this study (Figure 1C-E). Among the lactobacilli, the probiotic strain, *L. reuteri* RC-14 had the lowest adhesion force to the cells, supporting the clinical finding of being unable to persist in the vaginal environment[8] and of *L. reuteri* species to be rare and transient colonizers[9,10]. This pattern of 'stickiness' may show a way forward to investigate vaginal biofilm structure and composition through the adhesion forces of relevant vaginal strains.

It is known from literature that bond maturation between an adhering bacterium and the epithelium involves membrane reorganization.

When a ligand comes into contact with the membrane, receptors are locally recruited and then stabilized via lipid rafts[11] and actin cytoskeletal elements[12]. Thus, we set out to manipulate the cell membrane and cytoskeleton to better understand their influence on bacterial adhesion. Previous research has shown that cells treated with methyl-β-cyclodextrin (MβCD) lose cholesterol from their membranes[13]. Treatment of the cell membrane with MβCD depleted almost 90% of the cholesterol from the VK2/E6E7 cells after 60 min of exposure (Figure 2).

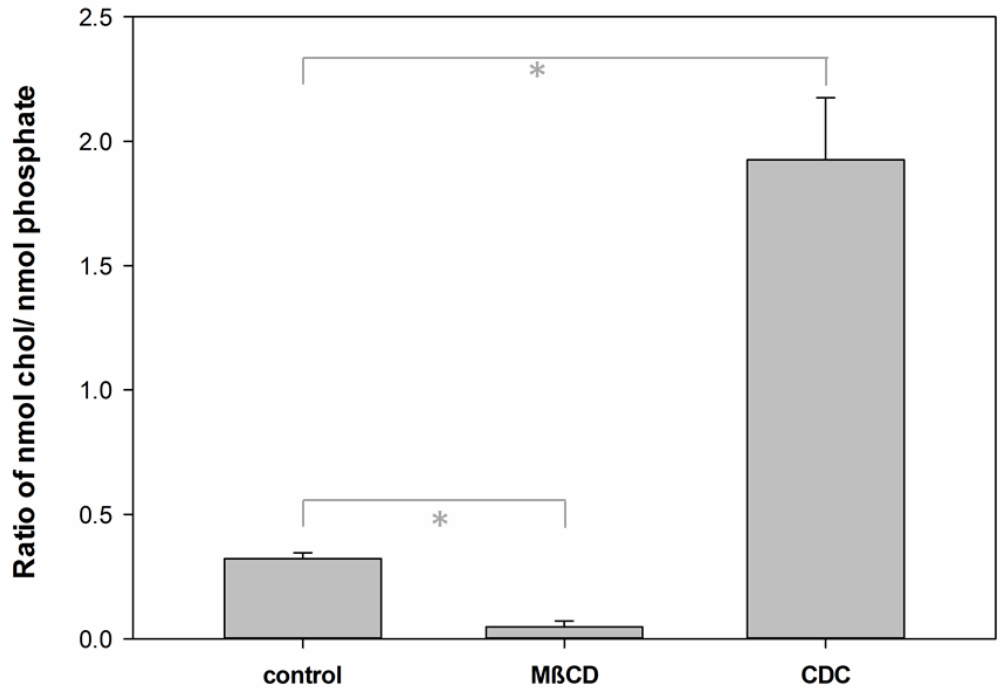

Figure 2 | Cholesterol depletion and repletion in VK2/E6E7 vaginal epithelial cells by MβCD and CDC.

VK2/E6E7 cells were untreated (control), treated with 10 mg/mL MβCD for 1 h (MβCD), or treated with 10 mg/mL MβCD for 1 h and then 10 mg/mL CDC for 1 h (CDC). The cells were then harvested and total membrane cholesterol relative to total lipid phosphate was determined. Data represent the means of three independent experiments. Statistical differences ($p<0.05$) are represented by an asterisk (*) as determined using the Student's *t* test.

The resultant interference in bacterial adhesion forces with *G. vaginalis* BME-1 was significant (solid green lines; Figure 3A, B) compared to the untreated cells (solid black lines) both to the membrane above the cytoplasm (-3.6 ± 0.9 nN versus -11.9 ± 0.3 nN) and the nucleus (-2.2 ± 0.5 nN versus -5.7 ± 0.3 nN). The cholesterol depletion was reversible for the membrane cholesterol levels (Figure 2) with cyclodextrin-cholesterol complex (CDC)[14] and the adhesion forces were equally recoverable (dashed green lines; Figure 3A, B) over both membrane sites (cytoplasm: -12.0 ± 0.3 nN; nucleus: -5.4 ± 0.5 nN). Upon further analysis (Figure 3C), we found that MβCD treatment moves the lipid raft marker Src out of the actin-dependent lipid raft fractions and to a lesser extent the actin-independent lipid raft fractions, as previously showed in other cell lines[15]. Src shifted back to the lipid raft fractions 1-2 and 3-4 upon cholesterol repletion using CDC. This indicates that the cholesterol effects on bacterial adhesion could be linked to lipid raft modulation. Interestingly, actin displayed similar behaviour, moving out of lipid raft fractions 1-2 upon MβCD treatment and this was also recoverable with CDC (Figure 3C).

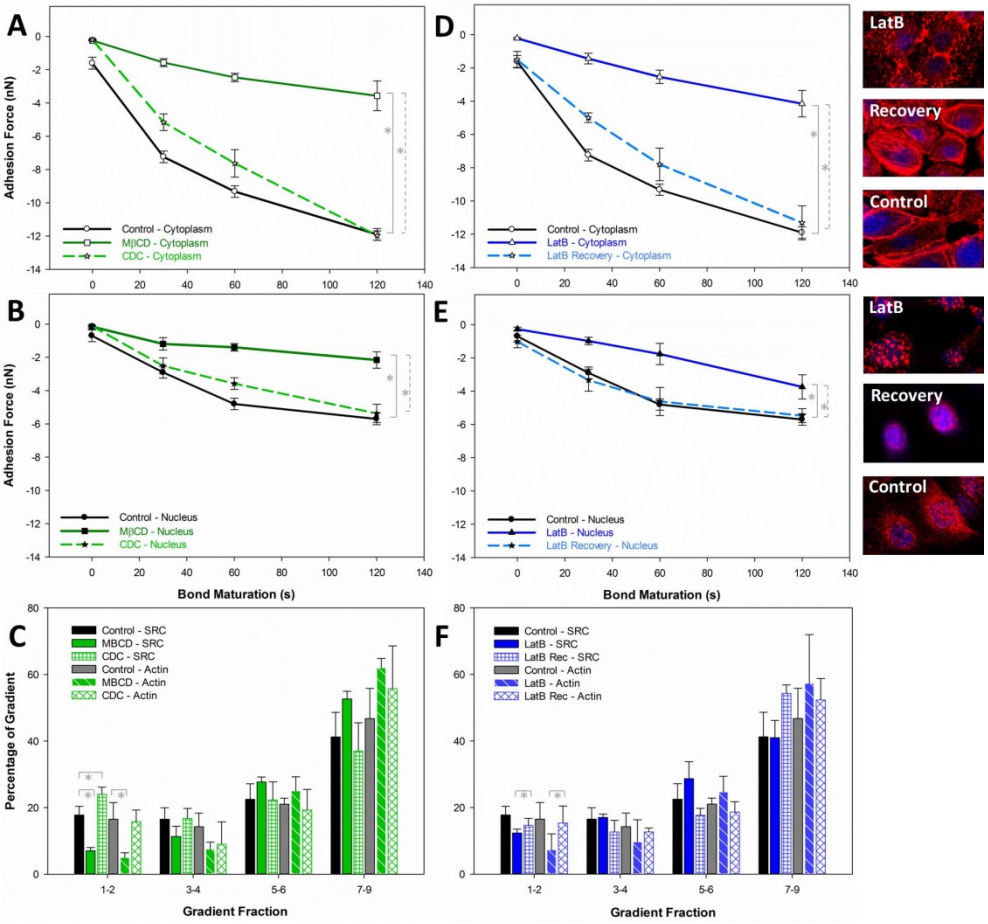

Figure 3 | The effect of cholesterol and actin inhibitors on localized bacterial adhesion between VK2/E6E7 cells and *G. vaginalis* BME-1 with AFM and lipid raft analysis.

A | Adhesion force measurements with *G. vaginalis* BME-1 on the membrane above the cytoplasm for untreated VK2/E6E7 cells (black line), cells treated with 10 mg/mL MβCD for 1 h (green line), and cells treated with 10 mg/mL MβCD for 1 h and then with 10 mg/mL CDC for 1 h (green dashed line). Data represents averages over a least 30 force-distance curves, measured on at least 6 different cells by three *G. vaginalis* probes with at least two different cultures per strain. Statistical differences ($p<0.05$) are represented by an asterisk (*) as determined by a Mixed Linear Model.

B | Same conditions as in **A** but measurements performed over the membrane above the nucleus. Untreated cells (black line), cells treated with MβCD (green line), and cells treated with MβCD and CDC (green dashed line).

C | VK2/E6E7 cells were treated with 10 mg/mL MβCD (or CDC) for 1 h and subjected to lipid raft analysis as previously described[15]. Src and actin markers were determined in the pooled gradient fractions 1–2, 3–4, 5–6, and 7–9 and were expressed as percentages of total src or actin in all fractions; fractions 1-2 (actin-dependant membrane lipids); fractions 3-4 (actin-independent membrane lipids). Data represent the means of three independent experiments. Statistical differences ($p<0.05$) are represented by an asterisk (*) as determined using the Student's *t* test.
D | Same conditions as in **A**, but adhesion force measurements were taken on the membrane above the cytoplasm for untreated cells (black line), cells treated with 10 µM LatB for 35 min (blue line), and cells treated with 10 µM LatB for 35 min and allowed to recover for 144 h (blue dashed line). Confocal laser scanning microscopy images to the right of the graph represent each of the conditions stained with both DAPI (blue – nucleus) and phalloidin (red – actin cytoskeleton) for observations of cell morphology (control cells, cells treated with 10 µM LatB, and cells recovered from LatB treatment after 144 h).
E | Same conditions as in **D** but measurements performed over the membrane above the nucleus. Untreated cells (black line), cells treated with 10 µM LatB (blue line), and cells treated with 10 µM LatB (blue dashed line).
F | Same conditions as in **C** but for untreated cells, cells treated with 10 µM LatB for 35 min, and cells treated with 10 µM LatB and then allowed to recover for 144 h.

Considering that the actin network has an effect on lipid raft stability and dynamics[16-18], we modulated the actin cytoskeleton and measured the effects on bacterial adhesion force. Latrunculin B (LatB) breaks down existing actin chains and prevents the formation of new actin polymers[19]. We disrupted the actin cytoskeleton with LatB for both the cytoplasm and the nucleus, resulting in a loss of adhesion force for *G. vaginalis* BME-1 (-4.1 ± 0.8 nN and -3.7 ± 0.7 nN, respectively). After allowing the actin cytoskeleton to recover, the adhesion force came nearly back to the control levels (-11.3 ± 1.0 nN and -5.5 ± 0.4 nN, respectively) (Figure 3D, E; CLSM images in the right panels), and confirmed the movement of actin out of and

back into actin-dependent lipid raft (fractions 1-2) upon actin disruption with LatB and recovery, respectively (Figure 3F).

Since a long recovery time of 144 h was needed for the cells crippled by LatB to regain their maximal adhesion force (Figure 3D, E), probably due to drastic cytoskeleton reorganizations, we used a second actin inhibitor to confirm these findings. Using Cytochalisin D, which only breaks down existing actin polymers[19], we achieved very similar results to LatB (Figure 4) in terms of adhesion force disruption and recovery, but with considerably less time needed for recovery. Taken together, optimal bacterial adhesion force requires both intact cellular cholesterol levels and an intact actin network.

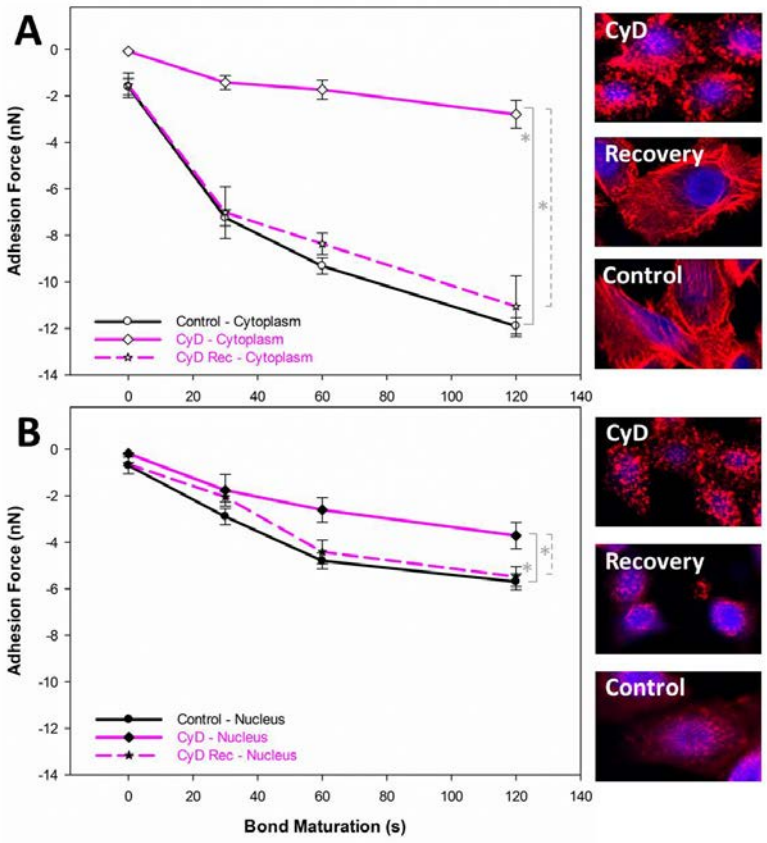

Figure 4 | Use of the actin inhibitor cytochalasin D to determine the effect on localized bacterial adhesion between VK2/E6E7 cells and *G. vaginalis* BME-1 with AFM.

A | Adhesion force measurements on the membrane above the cytoplasm for untreated cells (black line), cells treated with 10 µg/mL CyD for 1 h (pink line), and cells treated with 10 µg/mL CyD for 1 h and allowed to recover for 24 h (pink dashed line). Data represent averages over a least 30 force-distance curves, measured on at least 6 different cells by three *G. vaginalis* probes with at least two different cultures per strain. Statistical differences ($p<0.05$) are represented by an asterisk (*) as determined by a Mixed Linear Model. Confocal laser scanning microscopy images to the right of the graph represent each condition (control cells, cells treated with 10 µg/mL CyD, and cells allowed to recover from CyD treatment) stained with DAPI (blue – nucleus) and phalloidin (red - actin cytoskeleton).

B | Same as in **A** but with measurements performed over the membrane above the nucleus for untreated cells (black line), cells treated with 10 µg/mL CyD for 1 h (pink line), and cells treated with 10 µg/mL CyD for 1 h and allowed to recover for 24 h (pink dashed line).

Lipid rafts that are stabilized by cholesterol likely play a role in the adhesion event, as evidenced by disruption and recovery of lipid rafts upon MβCD treatment and CDC treatment, respectively. Lipid raft stability does not appear to strictly depend on actin for this cell line, as Src does not move out of lipid raft fractions upon LatB treatment (Figure 3F). More likely, the actin network is involved in lipid raft dynamics, which in turn is required for optimal bacterial adhesion forces. This may involve merger of lipid rafts into larger platforms at the site of bacterial adhesion, allowing the recruitment and stable binding of cellular receptors for bacterial ligands.

Our results indicate that the epithelial cells actively create sticky membranes to coordinate initial bacterial adhesion through cholesterol-dependent lipid rafts and the actin cytoskeletal network. Over time this allows bacteria to adhere strongly at the membrane surface, which is reflected in the bond maturation of the bacteria (Figure 1D, E). Apparently bond maturation develops differently over the two membrane locations. It could be that the lateral recruitment of receptors is more efficient above the cytoplasm, although both cholesterol-dependent lipid rafts and actin are involved in this process at both sites. We suggest that lipid rafts could be a limiting factor in bacterial adhesion, based on measurement of the cholesterol/protein ratio in cell homogenates. VK2/E6E7 cells showed a considerably lower ratio (0.023 nmol cholesterol/µg protein) compared to two other cell lines, Neuro-2A (0.041 nmol cholesterol/µg protein) and BHK (0.050 nmol cholesterol/µg protein), both of which have established actin-stabilized lipid rafts[20]. Replenishment of cholesterol with CDC to very high levels (Figure 2) confirms the notion of relatively low intrinsic levels of cholesterol in VK2/E6E7 cells. The cells may inhibit the recruitment of

receptors in the immediate vicinity of the nucleus to conserve the membrane space around this organelle for maintenance of the nucleus position[21].

The cholesterol and actin experiments provide a clear mechanism for bond maturation, albeit cannot fully explain our original observation of preferential adhesion. Biophysical experiments shed more light on this: we observed a prominent nucleus (Figure 5A) that was topographically distinct at the membrane (Figure 5B). Furthermore, the least adhesive location on the cell membrane was found to be above the nucleus (Figure 5B), as well as the stiffest (Figure 5D).

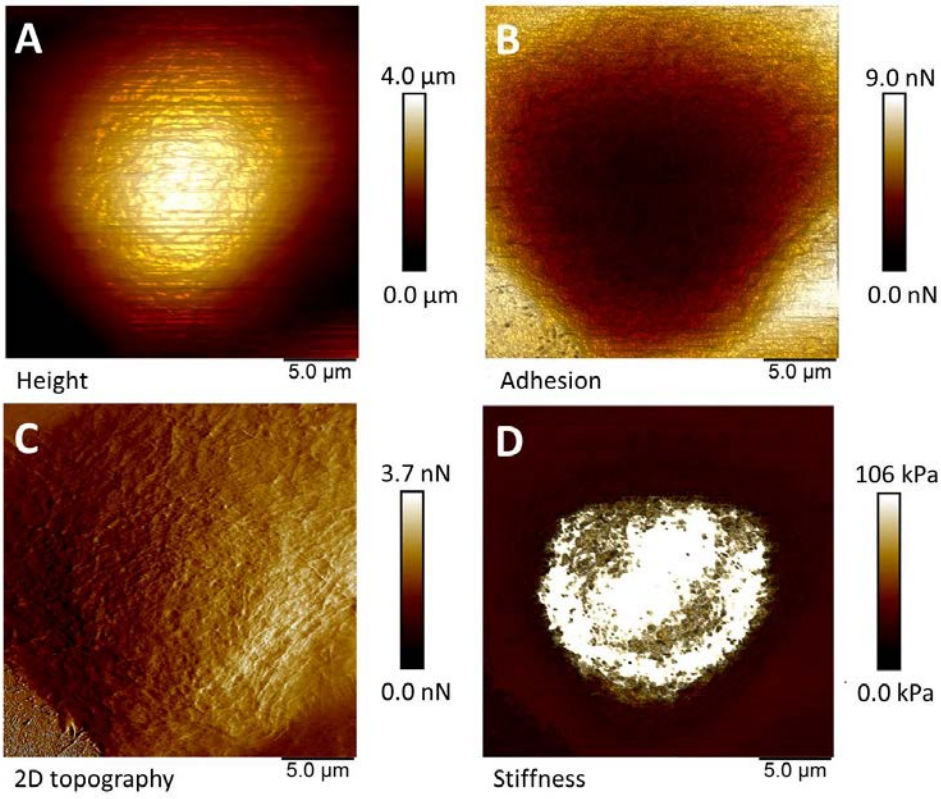

Figure 5 | Biophysical exploration of VK2/E6E7 vaginal epithelial cells by AFM.

A | *AFM height map of a VK2/E6E7 cell*. The scanning area was 20 x 20 µm and the image was obtained using PeakForce Mode in PBS. Lighter colouring indicates higher areas in terms of height than the darker parts of the cell.

B | *AFM adhesion force map*, showing adhesion to the cantilever of the same cell as in **A**; lighter areas are more adhesive to the probe than darker areas.

C | *2D surface topography map* (performed with Peak Force Error) of a VK2/E6E7 cell, the same cell as **A**.

D / *Stiffness map* (shown by the Sneddon Modulus) of the same cell as in **A**; lighter areas are more stiff than darker areas.

Decreasing stiffness may indicate a greater ability to conform to adhering bacteria, thereby strengthening bonds through more interactions. Membrane adhesion is orchestrated by the coordination of receptors and the process of bacterial binding to certain receptors can form temporary

large clusters[22,23]. The fact that there is such a marked difference in adhesion and stiffness may suggest unique local membrane composition and recruitment.

Based on our findings, we propose a model whereby bacterial adhesion to the cell membrane is initially regulated largely by the cell itself (Figure 6). The cell modulates local cholesterol to stabilize lipid rafts and recruits the actin cytoskeleton to allow lipid raft dynamics, all meant to recruit lipid raft-associated receptors to the adhesion site.

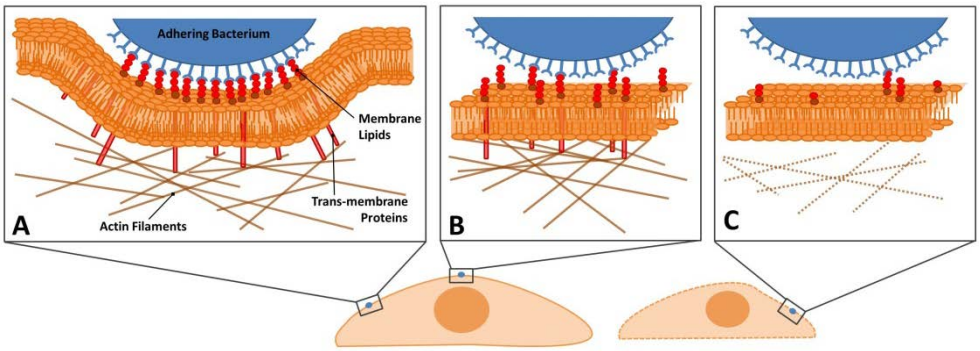

Figure 6 | Hypothetical model by which VK2/E6E7 cells direct initial bacterial adhesion at their membrane surfaces.

A | *Bacterial adhesion to membrane area above cytoplasm*. The cell membrane above the cytoplasm is able to deform to the bacteria and the lipid rafts and actin cytoskeleton work in concert to recruit local membrane receptors to maximally bind to the bacterial ligands, thereby creating strong adhesion forces between the two organisms.

B | *Bacterial adhesion to membrane area above nucleus*. The membrane has limited binding capacity due in part to the stiffness of the membrane and difficulty to deform and mold to the adhering bacterium, which results in a decreased number of focal binding points between the adhering bacterium and the cell, compared to adhesion above the cytoplasm.

C | *Bacterial adhesion to a cell with a membrane depleted in cholesterol and a disrupted actin cytoskeleton.* Membrane loses its sensitivity to adhering bacteria as strong adhesion forces are inhibited due to the lack of cholesterol in the membrane (lipid raft stabilizing and receptor recruiting defects) and the loss of the actin cytoskeletal connections below (lipid raft dynamics and membrane shape defects).

We have demonstrated that the membrane above the cytoplasm is the preferential site for bacterial adhesion, possibly to ensure adequate space for local membrane events (e.g. signalling[24], cell motility[25], protein and lipid uptake[26]). This model does not rule out a role for bacteria in the adhesion process; it suggests rather that the bacteria themselves may take over a larger part of the subsequent colonization and thus influence biofilm composition over time. Future work could focus on understanding the molecular events that occur in the cell upon immediate bacterial binding, to see if there is potential for therapeutic application targeting the cell. In addition, cellular changes that enhance commensal and probiotic lactobacilli colonization and metabolic activity, for example increasing HDL cholesterol[27], are worth exploring to reduce the many infections suffered by women[28,1].

Methods

Bacterial strains and culture conditions

E. coli C1214, and *S. aureus* MN8 were cultured and maintained aerobically in brain heart infusion (BHI, OXOID, Basingstoke, UK) broth and *G. vaginalis* BME-1 (clinically isolated from a BV patient) was cultured and maintained anaerobically in BHI medium at 37°C. *L. reuteri* RC-14, *L. iners* AB-1 and *L. crispatus* 33820 were cultured anaerobically in de Mann, Rogosa and Sharpe (MRS, MERCK, Darmstadt, Germany) broth at 37°C. For all experiments, main cultures of all bacterial strains were harvested by centrifugation for 5 min at 5000 *g*, washed twice with phosphate buffered

saline (PBS, 10 mM potassium phosphate and 140 mM NaCl, pH 7.0) and resuspended either in PBS or in the appropriate growth medium.

Vaginal epithelial cell line and culture conditions

The VK2-E6E7 cell line (ATCC®CRL-2616TM) was cultured and maintained in keratinocyte serum-free medium (KSFM) supplemented with 50 mg/mL bovine pituitary extract and 0.1 ng/mL epidermal growth factor. The cells were grown at 37°C with 5% CO2 and 100% humidity. Briefly, the cells were grown in T75 culture flasks, medium was renewed every 2-3 days, and the cells passaged after 80-85% confluence was achieved. Trypsin was added to detach the cells at 37°C and upon detachment of the cells, 1:1 Dulbecco's modified Eagle's medium and Ham's F12 medium containing 10% fetal bovine serum was added to neutralize the trypsin. The cells were then centrifuged for 5 min at 800 *g*, the supernatant was discarded and the pellet was resuspended in KSFM.

Adhesion assays

For the adhesion experiments, cells were seeded onto 12-well plates and grown until confluent. The bacteria were re-suspended to a final concentration of 1.0 x 10^5 bacteria/mL in KSFM and allowed to adhere to a monolayer of VK2/E6E7 cells for 1 h. Then, the cells and bacteria were washed three times with sterile PBS and fixated in 3.7% paraformaldehyde and dehydrated in ethanol prior to embedding. Each sample was embedded in methyl-acrylate and 2 µm-thick sections were cut prior to staining with toluidine blue. Following the staining, the samples were imaged using a Leica DM4000B microscope and quantified by counting all bacteria directly adhering to the cell membrane above the nucleus and those adhering to the

membrane above the cytoplasm. A total of at least 80 cells were counted for each sample, using 3 separate cell passages and at least 3 different bacterial cultures.

Bacterial adhesion forces

In order to measure bacterial adhesion forces using AFM, bacteria were immobilized to the D tip of an O-NP silicon nitride cantilever coated with 0.1% w/v poly-L-lysine (Sigma-Aldrich, Zwijndrecht, The Netherlands) from a suspension of 1.0 x 10^5 bacteria/mL in PBS. VK2/E6E7 cells were seeded onto 35 mm tissue culture dishes (Greiner, Frickenhausen, Germany) and grown until confluent. Adhesion forces between a bacterial probe and the epithelial layer were measured using a Nanoscope V (Digital Instruments, Woodbury, USA) under a 1.0 nN trigger threshold after a contact time of 120 s and the maximal adhesion force upon retraction was recorded.

Lipid raft analysis

To determine the effect of cholesterol depletion/repletion and actin disruption on lipid rafts, 10 mg/mL of MβCD in KSFM, 10 mg/mL MβCD followed by 10 mg/mL CDC (described below), or 10 mM solution of LatB in KSFM were added to a confluent 75 cm^2 flask of cells for 1 h and incubated in 37°C. A detergent-free raft isolation method developed by Macdonald and Pike[29] was used. In this procedure, confluent cells of two 75 cm^2 flasks were washed and subsequently scraped in base buffer (20 mM Tris/HCl, pH 7.8, and 250 mM sucrose) supplemented with 1 mM $CaCl_2$ and 1 mM $MgCl_2$. The harvested cells were centrifuged at 250 *g* for 5 min and the resulting pellet was suspended in 1 mL of base buffer supplemented with 1 mM $CaCl_2$,

1 mM $MgCl_2$ and protease inhibitors. After homogenization by passage through a 25-gauge needle 20 times, another centrifugation step at 1000 *g* for 10 min followed. The resulting post-nuclear supernatant (PNS) was collected and transferred to a separate tube. The pellet was homogenized again in 1 mL of base buffer supplemented with 1 mM $CaCl_2$, 1 mM $MgCl_2$ and protease inhibitors, passed through the needle 20 times and centrifuged at 1000 *g* for 10 min. The second PNS was combined with the first. Protein content of the combined PNS was determined using the detection reagent bicinchoninic acid, which forms purple complexes with Cu^{1+} in an alkaline environment. This generates a chromophore-based analytical method able to measure the amount of Cu^{1+} produced in the reaction of protein with alkaline Cu^{2+} [30]. Samples containing equal amounts of protein and adjusted to volumes of 2 mL were processed for gradient analysis. Subsequently, 2 mL of base buffer containing 50% OptiPrep was added to the PNS solution. By using a gradient mixer, an 8 mL gradient of 0-20% OptiPrep in base buffer was poured on top of this 4 mL in a centrifugation tube. After centrifugation at 52000 *g* for 90 min at 4°C, 9 fractions of 1.3 mL were collected from top to bottom and stored at -20°C.

For immunoblot analysis, protein from equal volumes of the gradient fractions were trichloroacetic acid precipitated and resuspended in sample buffer (5% SDS, 5% β-mercaptoethanol, 0.125 M Tris-HCl, pH 6.8, and 40% glycerol). The samples were resolved on SDS-polyacrylamide gel electrophoresis and subsequently electrotransferred onto a polyvinylidene fluoride membrane. After blocking of the membranes with Odyssey blocking buffer/PBS, the membranes were incubated with a primary antibody against c-Src (Santa Cruz Biotechnology, Santa Cruz, CA, U.S.A.) or actin (Sigma, St.

Louis, MO, U.S.A.). After washing incubation with the appropriate infrared fluorescent dye-conjugated secondary antibody, the washed immunoblots were scanned with the Odyssey (LI-COR Biosciences, Lincoln, NE, U.S.A.) and the fluorescence was measured. Relative quantification was performed using the Odyssey software. For each protein we calculated the percentage found in each gradient fraction relative to the total of that protein, which is the sum of the values of all gradient fractions. In addition, the 9 fractions were pooled as follows: 1-2, 3-4, 5-6, 7-9.

Cholesterol modulation and determination

To deplete cholesterol (used for AFM experiments and raft analysis), the cells were treated with 10 mg/mL MβCD in KSFM for 1 h at 37°C. For cholesterol loading of the plasma membrane for all experiments, MβCD loaded with cholesterol (CDC) was used at a concentration of 10 mg/mL in KSFM, for 1 h at 37°C. To prepare CDC, 100 mg of MβCD was dissolved in 2 mL of water and 3 mg of cholesterol (solution in ethanol) was added slowly while stirring at 60-70°C. This was dried and dissolved in KSFM. The AFM experiments (either for MβCD or CDC) continued with two washing steps in sterile PBS (37°C) and then measurements began in sterile PBS at 37°C.

To determine the amount of cholesterol depletion and repletion after incubation with MβCD respectively MβCD/CDC, the cells were harvested by trypsinization and the protein content was measured using the method as mentioned above. Then from the total cell homogenate, the lipids were extracted. In the extract, the cholesterol content was determined spectrophotometrically using a cholesterol/peroxidase assay[31].

The phosphorus content, as a measure for the phospholipid content, was determined using a phosphate assay[32].

The effect of the actin and cholesterol inhibitors on the morphology of VK2/E6E7 cells

VK2/E6E7 cells were seeded onto fibronectin-coated (25 µg/mL) 16 mm sterilized glass coverslips and grown to 80-90% confluence in the conditions as described above. Then one of each of the inhibitors (10 mg/mL MβCD for 1 h, 10 mg/mL CDC for 1 h, 10 µM LatB for 35 min, or 10 µg/mL CyD for 1 h) were applied to the cells in KSFM, in addition to an untreated condition. Following this, the cells were thoroughly washed with PBS and fixated with 3.7% paraformaldehyde. After fixation, the samples were rinsed with PBS and stained for 30 min with 4 µg/mL of DAPI and 2 µg/mL of TRITC-Phalloidin. Each sample was then inverted and mounted onto a glass slide with Vectashield® medium for fluorescence (Vector Laboratories, Inc. Burlingame CA 94010, USA) and then sealed. Slides were examined by confocal laser scanning microscopy using a LEICA TCS SP2 system (Leica Microsystems Heidelberg GmbH, Heidelberg, Germany). Confocal images were obtained using a 63x oil immersion objective at randomly chosen locations on the slides with 1.5 µm steps in the z-direction and images were stacked to provide an overlay image of the monolayer.

Statistical analysis

The inter- and intra-bacterial statistical differences in maximal adhesion forces on two membrane locations for each of the strains in Figure 1D, E were determined using a linear mixed effects model (LMM). Our null hypothesis was that there were no differences between bacteria at either

membrane location and furthermore, that there were no differences between membrane locations for any individual bacterium. This model also determined the intra-bacterial locational differences for *G. vaginalis* with the use of inhibitors on each of the membrane locations. The null hypothesis here was that the use of LatB, MβCD, and CDC had no effect on the maximal adhesion forces compared to the control of unaffected cells with a *G. vaginalis* BME-1 probe at either membrane location. The LMM accounted for random variations due to the differences in adhesion forces for fixed combinations (e.g. VK2/E6E7-*E. coli*), including the use of multiple bacterial cultures and probes. Then, procedure MIXED of SAS (Version 9.2) using a restricted maximum likelihood and the Kenward-Rogers option for the number of degrees of freedom was used to fit the LMM. This yielded modelled values of the mean adhesion forces, representing the maximal adhesion force from the interaction of each pair.

The lipid raft data is represented in all figures as mean ± standard deviation (SD) and the control and inhibitor data were analyzed using a two-tailed Student's *t* test parametric tests using p-values of <0.05 as statistically significant. The null hypothesis was that the inhibitors (MβCD, CDC, and LatB) had no effect on the overall amount of Src and actin in each of the gradient fractions compared to the control values.

References

1. van de Wijgert, J. H. H. M. *et al*. The vaginal microbiota: what have we learned after a decade of molecular characterization? *PLoS ONE* 9, e105998 (2014).
2. Canny, G. O. & McCormick, B. A. Bacteria in the intestine, helpful residents or enemies from within? *Infect. Immun*. 76, 3360-3373 (2008).
3. Pizarro-Cerdá, J. & Cossart, P. Bacterial adhesion and entry into host cells. *Cell* 124, 715-727 (2006).
4. Beaussart, A. *et al*. Quantifying the forces guiding microbial cell adhesion using single-cell force spectroscopy. *Nature Protocols* 9, 1049-1055 (2014).
5. Liu, Y., Pinzón-Arango, P. A., Gallardo-Moreno, A. M. & Camesano, T. A. Direct adhesion force measurements between *E. coli* and human uroepithelial cells in cranberry juice cocktail. *Mol. Nutr. Food. Res.* 54, 1744-1752 (2010).
6. Machado, A., Salgueiro, D., Harwich, M., Jefferson, K. K. & Cerca, N. Quantitative analysis of initial adhesion of bacterial vaginosis-associated anaerobes to ME-180 cells. *Anaerobe* 23, 1-4 (2013).
7. Swidsinski, A. *et al*. Adherent biofilms in bacterial vaginosis. *Obstet. Gynecol*. 106, 1013–1023 (2005).
8. Gardiner, G. E., Heinemann, C., Bruce, A. W., Beuerman, D. & Reid, G. Persistence of *Lactobacillus fermentum* RC-14 and *Lactobacillus rhamnosus* GR-1 but not *L. rhamnosus* GG in the human vagina as demonstrated by randomly amplified polymorphic DNA. *Clin. Diagn. Lab. Immunol.* 9, 92–96 (2002).
9. Hummelen, R. *et al*. Deep Sequencing of the Vaginal Microbiota of Women with HIV. *PLoS ONE* 5, e12078 (2010).
10. Ravel, J. *et al*. Vaginal microbiome of reproductive-age women. *Proc. Natl. Acad. Sci. USA*. 15, 4680-4687 (2011).
11. Sánchez-Wandelmer, J. *et al*. Inhibition of cholesterol biosynthesis disrupts lipid raft/caveolae and affects insulin receptor activation in 3T3-L1 preadipocytes. *Biochim. Biophys. Acta*. 1788, 1731-1739 (2009).
12. Chichili, G. R. & Rodgers, W. Clustering of membrane raft proteins by the actin cytoskeleton. *J. Biol. Chem.* 282, 36682-36691 (2007).
13. Yancey, P. G. *et al*. Cellular cholesterol efflux mediated by cyclodextrins. Demonstration of kinetic pools and mechanism of efflux. *J. Biol. Chem*. 271, 16026-16034 (1996).
14. Christian, A. E., Haynes, M. P., Phillips, M. C. & Rothblat, G. H. Use of cyclodextrins for manipulating cellular cholesterol content. *J. Lipid. Res*. 38, 2264-2272 (1997).
15. Klappe, K., Hummel, I. & Kok, J. W. Separation of actin-dependent and actin-independent lipid rafts. *Anal. Biochem*. 438, 133-135 (2013).
16. Head, B. P. *et al*. Microtubules and actin microfilaments regulate lipid raft/caveolae localization of adenylyl cyclase signaling components. *J. Biol. Chem*. 281, 26391-26399 (2006).
17. Kok, J. W. *et al*. Are lipid rafts involved in ABC transporter-mediated drug resistance of tumor cells? *TIGG*. 20, 373-397 (2008).
18. Chichili, G. R. & Rodgers, W. Cytoskeleton-membrane interactions in membrane raft structure. *Cell. Mol. Life. Sci*. 66, 2319-2328 (2009).
19. Wakatsuki, T., Schwab, B., Thompson, N. C. & Elson, E. L. Effects of cytochalasin D and latrunculin B on mechanical properties of cells. *J. Cell. Sci*. 114, 1025-1036 (2001).
20. Hummel, I., Klappe, K., Ercan, C. & Kok, J. W. Multidrug resistance-related protein 1 (MRP1) function and localization depend on cortical actin. *Mol. Pharmacol*.79, 229-240 (2009).
21. Dahl, K. N. & Kalinowski, A. Nucleoskeleton mechanics at a glance. *J. Cell. Sci*. 124, 675-678 (2011).

22. Triantafilou, M. *et al*. Combinational clustering of receptors following stimulation by bacterial products determines lipopolysaccharide responses. *Biochem. J.* 381, 527–536 (2004).
23. Bethani, I., Skånland, S. S., Dikic, I. & Acker-Palmer, A. Spatial organization of transmembrane receptor signalling. *EMBO J*. 29, 2677-2688 (2010).
24. Simons, K. & Toomre, D. Lipid rafts and signal transduction. *Nat. Rev. Mol. Cell*. Biol. 1, 31-39 (2000).
25. Gómez-Móuton, C. *et al*. Segregation of leading-edge and uropod components into specific lipid rafts during T cell polarization. *Proc. Natl. Acad. Sci. USA*. 98, 9642-9647 (2001).
26. Pelkmans, L., Bürli, T., Zerial, M. & Helenius, A. Caveolin-stabilized membrane domains as multifunctional transport and sorting devices in endocytic membrane traffic. *Cell* 118, 767-780 (2004).
27. Mohamadshahi, M. *et al*. Effects of probiotic yogurt consumption on lipid profile in type 2 diabetic patients: A randomized controlled clinical trial. *J. Res. Med. Sci.* 19, 531-536 (2014).
28. Reid, G. *et al*. Microbiota restoration: natural and supplemented recovery of human microbial communities. *Nat. Rev. Microbiol*. 9, 27–38 (2011).
29. Macdonald, J. L. & Pike, L.J. A simplified method for the preparation of detergent-free lipid rafts. *J. Lipid. Res*. 46, 1061-1067 (2005).
30. Smith, P. K. *et al*. Measurement of protein using bicinchoninic acid. *Anal. Biochem*. 150, 76-85 (1985).
31. Gamble, W., Vaughan, M., Kruth, H. S. & Avignan, J. Procedure for determination of free and total cholesterol in micro- or nanogram amounts suitable for studies with cultured cells. J. *Lipid. Res.* 19, 1068–1070 (1978).
32. Böttcher, C. J. F., van Gent, C. M. & Pries, C. A rapid and sensitive sub-micro phosphorus determination. *Anal. Chim. Acta*. 24, 203–204 (1961).

Acknowledgements

This work was supported by the University Medical Center Groningen, The Netherlands. HJB is also director of a consulting company, SASA BV (GN Schutterlaan 4, 9797 PC Thesinge, The Netherlands). The authors declare no potential conflicts of interest with respect to authorship and/or publication of this article. Opinions and assertions contained herein are those of the authors and are not construed as necessarily representing views of their respective employers. The authors would like to thank D. Hoekstra for valuable discussions and insight, and M. B. M. van Leeuwen for the idea for histology experiments and for performing the sample embedding and histology.